

This is the accepted manuscript made available via CHORUS. The article has been published as:

Tight-binding study of hcp Zn and Cd

X. W. Sha, D. A. Papaconstantopoulos, M. J. Mehl, and N. Bernstein

Phys. Rev. B **84**, 184109 — Published 28 November 2011

DOI: [10.1103/PhysRevB.84.184109](https://doi.org/10.1103/PhysRevB.84.184109)

Tight-binding study of hcp Zn and Cd by the NRL-TB method

X. W. Sha, D. A. Papaconstantopoulos

School of Physics, Astronomy, and Computational Sciences, George Mason University,
Fairfax, Virginia 22030, USA

M. J. Mehl, and N. Bernstein

Center for Computational Materials Science, Naval Research Laboratory, Washington,
DC 20375, USA

We have developed tight-binding Hamiltonians for the hcp transition metals zinc and cadmium based on the Naval Research Laboratory Tight-Binding (NRL-TB) method. The Hamiltonians have a nonorthogonal basis and are derived by fitting to band structures and total energies of first-principles linearized augmented plane wave calculations. We have applied this approach to compute the ground state behavior, phase stability, band structures, densities of states, elastic moduli, and phonon frequencies for both Zn and Cd, and have found good agreement with available experimental and theoretical data in most cases. This approach also enables us to perform large-scale molecular dynamics simulations to calculate the vacancy formation energies, atomic mean square displacements and coefficients of thermal expansion, at a small fractional cost of computational times compared with first-principles techniques.

PACS number(s): 71.15.Ap, 71.15.Nc, 71.20.-b, 71.15.Pd

I. Introduction

The Naval Research Laboratory Tight-Binding (NRL-TB) method is based on the two-center Slater-Koster^{1, 2} formulation of tight-binding with a nonorthogonal basis, taking advantage of the fact that the density functional theory^{3, 4} allows an arbitrary shift in the potential,^{5, 6} which makes it possible to fit the total energy without employing an empirical potential. The form of the NRL-TB parameters allows excellent transferability to different crystal structures and atomic configurations, and has been successfully applied to examine various structural, electronic, energetic and dynamical properties of many transition and noble metals,⁵⁻¹⁸ semimetals,¹⁹ heavy metals,²⁰ semiconductors,²¹⁻²³ alloys,²⁴⁻²⁷, carbon nanostructures,²⁸⁻³⁰ and metal oxides³¹⁻³³, etc. In particular, NRL-TB Hamiltonians have been previously developed for all the transition metals, except for column IIB. Here we applied the NRL-TB method to the hcp transition metals zinc and cadmium. Both Zn and Cd differ significantly from the typical transition metals that have a low lying s-band and another five d-bands that progressively fill up so that the Fermi level (E_f) is either within the d-bands or just above for the noble metals. On the contrary, Zn and Cd have deep d-bands which fall between the first predominantly s-like band and a seventh band with s-p character crossed by E_f . The situation is also different from some free-electron metals such as Al that have no occupied d-bands. In contrast to most hcp metals, Zn and Cd have unusually large axial ratios which are well above the ideal hcp ratio³⁴ and thus have some unique material properties such as the lowest melting points in transition metals aside from mercury. In section II we detail the theoretical methods used to develop the NRL-TB Hamiltonians and perform tight-binding molecular dynamics

simulations. In section III we present the results and related discussions on various tight-binding derived properties obtained from both the static calculations and molecular dynamics simulations, and conclude with a brief summary in Section IV.

II. Theoretical methods

In the two-center nonorthogonal NRL-TB scheme, the Slater-Koster terms include both the environment-dependent on-site parameters and the bond-length-dependent hopping parameters.^{5, 35} The on-site terms are assumed to be diagonal and have a polynomial form as a function of the atomic density. For a single element, the density of atom i is defined as

$$\rho_i = \sum_j \exp(-\lambda^2 R_{ij}) F_C(R_{ij}) \quad , \quad (1)$$

where the sum is over all the neighboring atoms j within a range of cutoff distance R_c of atom i , λ is a fitting parameter, and $F_C(R_{ij})$ is a smooth cut-off function. The angular-momentum-dependent on-site terms are defined by

$$h_\ell = a_\ell + b_\ell \rho^{\frac{2}{3}} + c_\ell \rho^{\frac{4}{3}} + d_\ell \rho^2 \quad , \quad (2)$$

where ℓ represents the s , p , and d orbitals, and a_ℓ, b_ℓ, c_ℓ and d_ℓ are our fitting coefficients.

We construct the two-center spd Slater-Koster hopping integrals from the ten independent SK parameters, which are assumed to all have polynomial times exponential forms in terms of neighbor distance

$$P_\gamma(R) = \sum_j (e_\gamma + f_\gamma R + g_\gamma R^2) \exp[-q_\gamma^2 R] F_c(R) \quad (3)$$

where γ indicates the type of interactions, including $ss\sigma$, $pp\sigma$, $sp\sigma$, $dd\sigma$, $sd\sigma$, $pd\sigma$, $pp\pi$, $dd\pi$, $pd\pi$, and $dd\delta$. R is the distance between the atoms, and e_γ , f_γ , g_γ , and q_γ are our

fitting coefficients. We define the Slater-Koster overlap functions in a non-orthogonal calculation to have the same form as the hopping parameters. Overall, there are in total 93 fitting coefficients for a single element in the on-site, hopping and overlap terms in the NRL-TB Hamiltonians with s , p , and d orbitals, and the values of these fitting coefficients for Zn and Cd are listed in Table I.

For both Zn and Cd, we used the full-potential Linearized Augmented Plane-Wave (LAPW) total energies^{36, 37} within the Local Density Approximation (LDA)⁴ to generate total energies and band structures for bcc, fcc, hcp and simple cubic crystal structures with varying atomic volumes, and, in the case of the hcp structure, we fitted only selected total energy values and not a full range of values and c/a ratios. The total energy is usually weighed at around 200-300 times over a single band energy. We are able to obtain fitting RMS error of less than 5 mRy and 0.2 mRy for the energy bands and total energy, respectively.

We calculate the finite-temperature dynamical properties from tight-binding molecular dynamics simulations, which are performed in the micro-canonical ensemble by integrating the equations of motion using Verlet's algorithm³⁸ and a time step of two femtoseconds. The forces on each atom are calculated from the eigenvectors of the TB Hamiltonian of the system using the Hellmann-Feynman theorem.³⁹ The supercells used in our molecular dynamics simulations contain 288 atoms, and we typically are able to approach equilibrium in the tight-binding molecular dynamics simulations within 2000 time steps (4 picoseconds).

III. Results and Discussion

1. Equilibrium Structure and Phase Stability

The NRL-TB method's combination of computational efficiency and transferability to different crystal structures and atomic configurations enable us to examine low-symmetry crystal structures and defect structures, in addition to the high-symmetry bcc, fcc, hcp and simple cubic phases used in the Hamiltonian fitting. In Table II, we list the calculated tight-binding total energies of Zn in 26 different crystal structures. Among all the structures examined, we find that the hcp structure is lowest in energy, consistent with experiment.³⁴ In Fig. 1(a) we show the volume dependence of the tight-binding total energies for fcc, bcc, simple cubic, hcp and diamond structures. The tight-binding calculations successfully reproduce the first-principles LAPW data of the fcc, bcc and simple cubic structures that are used in the development of the tight-binding Hamiltonians. For the hcp structure, we minimize the tight-binding total energies as a function of c/a ratio at each given volume, thus the tight-binding results are not directly comparable with the LAPW energies used in the tight-binding fitting due to the different c/a ratios. The equilibrium volume for hcp Zn is somewhat underestimated in tight-binding (91.23 bohr³/atom), in comparison to the experiment at 102.56 bohr³/atom.³⁴ This discrepancy is mainly due to the use of the LDA in our input database, which usually underestimates the equilibrium volume of the 3d transition metals.⁴⁰ In contrast, previous first principles calculations using generalized-gradient-approximation (GGA) predict an equilibrium volume of 97.32 bohr³/atom,⁴¹ in closer agreement with experiment. The tight-binding calculated c/a ratio at the equilibrium ($c/a=1.828$) is in good agreement with experiment ($c/a=1.856$), similar to previous first principles calculations.⁴¹ Our tight-binding calculations find no significant anomaly in the c/a ratio

for hcp Zn under compression, consistent with hydrostatic high-pressure powder x-ray diffraction experiments⁴² and first-principles calculations⁴³.

The tight-binding predicted equilibrium properties of Cd are quite similar to those of Zn. The hcp structure also has the lowest energy among the 26 different crystal structures examined, as shown in Table III and Fig. 1(b). The tight-binding calculations underestimate the hcp equilibrium volume by $\sim 6.5\%$, in comparison with the experimental value of 145.63 Bohr³/atom at ambient conditions, again due to the fitting of the Hamiltonians to LAPW calculations using the LDA approximation. The tight-binding calculations predict a c/a ratio of 1.883 in close agreement with equilibrium experimental value of 1.885, similarly to the Zn results.

The fact that the LDA results, to which our TB fit was based, are in better agreement with experiment for Cd than Zn is consistent with previous findings. Indeed the LDA results for the 4d metals agree better to the experiment than those for the 3d metals⁴⁴.

2. Electronic Structure

At the ambient experimental equilibrium volume, the tight-binding calculated band structure and electronic density of states are in excellent agreement with first-principles LAPW results for both hcp Zn and Cd, as shown in Fig. 2 and 3. For hcp Zn, the 3d bands are centered at ~ 0.58 Ry below the Fermi level and mostly confined within a narrow range of ~ 0.15 Ry. The 3d bands are located deeper in hcp Cd, at ~ 0.66 Ry below the Fermi level with a narrow distribution of ~ 0.15 Ry. For both hcp Zn and Cd, most bands around the Fermi level have mixed s and p character. Since the d-bands are

occupied and located far below the Fermi level, Zn and Cd should be viewed more like free-electron metals such as Mg, instead of as a typical transition metal, where d-bands are generally close to the Fermi surface and play an important role in bonding.

The tight-binding calculated Fermi surfaces of hcp Zn at the ambient experimental equilibrium volume are in close agreement with first-principles LAPW results, as shown in Fig. 4. There are three major bands shown in the Fermi surfaces, one forming pockets around the upper and lower parts of each corner (the H point in the Brillouin zone) (green/yellow); the second (purple/blue) filling the entire corner (along the K-H line) and possibly connecting the corners (it's hard to be certain even using 11,000 k-points); and the third, in light blue, filling the zone center. One noticeable difference between the tight-binding and LAPW surfaces can be found in the purple necks. In tight-binding the neighboring necks tend to connect to each other, while in LAPW there are no connections. Such differences can be also seen in the band structure, where the tight-binding band goes just above the Fermi level and the LAPW band goes just below it in the Σ direction. For hcp Cd, the tight-binding and LAPW calculated Fermi surfaces show better agreement, as shown in Fig. 5. There is no observable trend to connect the purple necks, and both tight-binding and LAPW predict the band energy below the Fermi level in the Σ direction.

3. Elastic Moduli

To calculate the elastic moduli, we impose volume-conserving external strains on the structure, relax any internal parameters to obtain the energy as a function of the strain, and numerically calculate the second derivative of the energy-strain curves.⁴⁵ As

shown in Table IV, in hcp Zn our tight-binding calculations significantly underestimate the bulk modulus and some of the elastic moduli (C_{13} , C_{33} , and C_{44}), all by over 20 GPa, in comparison to the experiment⁴⁶. The significant underestimation of C_{13} and C_{33} has been previously reported in density-functional theory calculations using both GGA and hybrid functionals for Zn⁴⁷. The calculated bulk and elastic moduli of hcp Cd show much better agreement with the experiment, all agree within 8 GPa.⁴⁶

4. Phonon Dispersion

Using the frozen phonon approximation,⁴⁸ we calculate the phonon dispersion curves along several high-symmetry directions in the Brillouin zone for both hcp Zn and Cd, as shown in Fig. 6. The phonon spectra were calculated using supercells generated by the PHON code⁴⁹ and Stokes's FROZSL code⁵⁰, the calculations agreeing well with each other. Since these calculations are performed at the equilibrium volume and c/a ratio predicted by the tight-binding Hamiltonians and the tight-binding equilibrium volume is significantly smaller than the experimental value, it is not surprising to see that the tight-binding calculated phonon frequencies for hcp Zn and Cd are mostly 10-20% higher than the inelastic neutron scattering measurements⁵¹. Phonon frequencies generally increase significantly with volume compression (increase of the pressure) in transition metals, as shown in many previous experimental and first-principles calculations^{45, 52-54}.

5. Atomic Mean Square Displacements

Atomic mean square displacement (MSD) is an important materials parameter to describe the lattice vibrational properties at finite temperatures.³⁸ We calculate the MSDs based on the time-dependent atomic coordinates obtained through tight-binding

molecular dynamics simulations at several selected temperatures.³⁸ The calculated MSDs for both hcp Zn and Cd show a linear increase with the increase of temperature, as shown in Fig. 7. Cd has a larger atomic MSD than Zn at all the temperatures we examined. We only report MSDs for Zn and Cd up to 500 K due to the low melting points of Zn (693 K) and Cd (594 K), and the fact that our tight-binding molecular dynamics simulations break when the temperature approaches the melting point. Our high-temperature tight-binding molecular dynamics simulations break at 750 K for Zn and 525 K for Cd, which are both close to the experimental melting points. The calculated MSD values of Cd agree well with the experimental data derived from the Debye-Waller factor measurements^{55, 56}, especially at around the ambient temperature. The increasing differences between the calculated and experimental values at higher temperatures are partially due to the fact that we perform all the molecular dynamics simulations at constant volume. The tight-binding calculations underestimated the MSD values of Zn, partially due to the underestimation of ambient equilibrium volume.

6. Coefficient of Thermal Expansion

The thermal expansion coefficient is a thermodynamic parameter that can also be obtained from our volume-conserving tight-binding molecular dynamics simulations at finite temperatures,¹¹

$$\alpha = \frac{1}{3B} \left(\frac{\partial P}{\partial T} \right)_V, \quad (4)$$

where B is the bulk modulus, P is the temperature-dependent pressure, and T is the temperature. We calculated P using the usual virial definition^{11, 18} by adding up both the potential and kinetic contributions, and found a linear temperature dependence for both

Zn and Cd, similar to that previously reported in several bcc transition metals.¹⁸ Zn and Cd are both highly anisotropic, due to the unusually large c/a ratios at their equilibrium hcp structures, so the experimentally measured linear thermal expansion coefficients vary significantly along the a and c axes. Our tight-binding calculated linear thermal expansion coefficients are in reasonable agreement with the average experimental values⁵⁷ (having the same order of magnitude), as shown in Table V.

7. Vacancy Formation Energy

The computational efficiency of our tight-binding method enables us to examine large supercells, such as defect structures with minimal defect-defect interactions. Point defects such as monovacancies are intrinsic at high temperatures and have significant impact on a materials' thermal and mechanical properties. The thermal concentration of vacancies is usually associated with the vacancy formation energy E_{vac} , which can be obtained from our tight-binding calculations using⁵

$$E_{\text{vac}}(V) = E_{\text{sc}}(N-1, 1; V) - (N-1)E_{\text{bulk}}(V/N) \quad (5)$$

where $E_{\text{sc}}(M, Q; V)$ is the total energy of a supercell with volume V containing M atoms and Q vacancies, and $E_{\text{bulk}}(V/N)$ is the total energy per atom for a bulk supercell of N atoms with volume V . When calculating the total energy for the vacancy-containing supercell, we ensure that the supercell is large enough to avoid the vacancy-vacancy interactions, and fully relax all the atoms using the conjugate gradient method while keeping the lattice symmetry. The calculated values are very sensitive to the supercell size and the number of k-points used in the tight-binding calculations. Using a supercell of $5 \times 5 \times 5$ which contains 249 metal atoms and one vacancy, we are able to obtain well

converged results of E_{vac} for both Zn and Cd when using 72 k-points in the tight-binding calculations, as shown in Table VI. In comparison to the experimental data measured from positron annihilation⁵⁸, our tight-binding calculation overestimated the E_{vac} for Cd and underestimated the value for Zn, by ~ 0.3 eV. Both hcp Zn and Cd have very low vacancy formation energies, roughly one order of magnitude smaller than many of the transition metals we previously studied.^{5, 18} As shown in the band structure, the occupied d bands in Zn and Cd are located deep below the Fermi level, and most bands around the Fermi level have mixed s and p character. Thus Zn and Cd have electronic structures more similar to free-electron metals than transition metals. Aluminum, one of the free-electron metals which is not far from Zn in the periodic table, is reported to have a vacancy formation energy of 0.6 eV⁵⁹, similar to the values of Zn and Cd.

IV. Conclusions

In summary, we have developed NRL-TB Hamiltonians for Zn and Cd by fitting to first-principles LAPW band structures and total energies within the LDA, and applied the Hamiltonians to compute the ground state behavior and phase stability, band structures, densities of states, elastic moduli, phonon frequencies, vacancy formation energies, mean square displacements, and thermal expansion coefficients. We examined the tight-binding energies of 26 different crystal structures including many low-symmetry and defect systems, and find that hcp has the lowest energy for both Zn and Cd. The tight-binding calculated band structure, density of states, and Fermi surfaces agree well with first-principles LAPW results. The tight-binding bulk and elastic moduli of hcp Cd are in excellent agreement with experiment, and tight-binding calculations underestimate the bulk modulus and several elastic moduli for hcp Zn. The phonon spectra, calculated using

the frozen phonon approximation, are in reasonable agreement with experiment. The calculated atomic mean square displacements increase linearly with temperature, and hcp Cd has a larger MSD value over Zn at all temperatures, in good agreement with the Debye-Waller factor measurements. The calculated linear thermal expansion coefficients agree with experiment. The vacancy formation energies of Zn and Cd are roughly one order of magnitude lower than most transition metals, but close to the formation energy of Aluminum.

Acknowledgments

Work at George Mason University was partially supported by grants DGE0638680 from NIST and N00014-09-1-1025 from ONR. Work at the Naval Research Laboratory was sponsored by the U.S. Office of Naval Research.

REFERENCES

- 1 J. C. Slater and G. F. Koster, Phys. Rev. **94**, 1498 (1954).
- 2 D. A. Papaconstantopoulos and M. J. Mehl, J. Phys.-Condes. Matter **15**, 413 (2003).
- 3 P. Hohenberg and W. Kohn, Phys. Rev. **136**, B864 (1964).
- 4 W. Kohn and L. J. Sham, Phys. Rev. **140**, A1133 (1965).
- 5 M. J. Mehl and D. A. Papaconstantopoulos, Phys. Rev. B **54**, 4519 (1996).
- 6 R. E. Cohen, M. J. Mehl, and D. A. Papaconstantopoulos, Phys. Rev. B **50**, 14694 (1994).
- 7 D. A. Papaconstantopoulos and M. J. Mehl, J. Phase Equilib. **18**, 593 (1997).
- 8 S. H. Yang, M. J. Mehl, and D. A. Papaconstantopoulos, Phys. Rev. B **57**, 2013 (1998).
- 9 F. Raouafi, C. Barreteau, M. C. Desjonqueres, and D. Spanjaard, Surf. Sci. **482**, 1413 (2001).
- 10 E. Z. da Silva, A. J. R. da Silva, and A. Fazzio, Phys. Rev. Lett. **87**, 256102 (2001).
- 11 F. Kirchhoff, M. J. Mehl, N. I. Papanicolaou, D. A. Papaconstantopoulos, and F. S. Khan, Phys. Rev. B **63**, 195101 (2001).
- 12 Y. Mishin, M. J. Mehl, D. A. Papaconstantopoulos, A. F. Voter, and J. D. Kress, Phys. Rev. B **63**, 224106 (2001).
- 13 M. J. Mehl, D. A. Papaconstantopoulos, Mazin, II, N. C. Bacalis, and W. E. Pickett, J. Appl. Phys. **89**, 6880 (2001).
- 14 M. J. Mehl and D. A. Papaconstantopoulos, Europhys. Lett. **60**, 248 (2002).
- 15 C. E. Lekka, M. J. Mehl, N. Bernstein, and D. A. Papaconstantopoulos, Phys. Rev. B **68**, 035422 (2003).
- 16 D. Finkenstadt, N. Bernstein, J. L. Feldman, M. J. Mehl, and D. A. Papaconstantopoulos, Phys. Rev. B **74**, 184118 (2006).
- 17 A. Shabaev and D. A. Papaconstantopoulos, Phys. Rev. B **79**, 064107 (2009).
- 18 C. E. Lekka, N. Bernstein, D. A. Papaconstantopoulos, and M. J. Mehl, Mater. Sci. Eng. B-Adv. Funct. Solid-State Mater. **163**, 8 (2009).
- 19 B. Akdim, D. A. Papaconstantopoulos, and M. J. Mehl, Philos. Mag. B-Phys. Condens. Matter Stat. Mech. Electron. Opt. Magn. Prop. **82**, 47 (2002).
- 20 M. Lach-Hab, B. Akdim, D. A. Papaconstantopoulos, M. J. Mehl, and N. Bernstein, J. Phys. Chem. Solids **65**, 1837 (2004).
- 21 N. Bernstein, M. J. Mehl, and D. A. Papaconstantopoulos, Phys. Rev. B **66**, 075212 (2002).
- 22 J. L. Feldman, N. Bernstein, D. A. Papaconstantopoulos, and M. J. Mehl, Phys. Rev. B **70**, 165201 (2004).
- 23 J. L. Feldman, N. Bernstein, D. A. Papaconstantopoulos, and M. J. Mehl, J. Phys.-Condes. Matter **16**, S5165 (2004).
- 24 D. A. Papaconstantopoulos and M. J. Mehl, Phys. Rev. B **64**, 172510 (2001).
- 25 S. H. Yang, M. J. Mehl, D. A. Papaconstantopoulos, and M. B. Scott, J. Phys.-Condes. Matter **14**, 1895 (2002).
- 26 C. E. Lekka, N. Bernstein, M. J. Mehl, and D. A. Papaconstantopoulos, Appl. Surf. Sci. **219**, 158 (2003).

27 C. E. Lekka, D. A. Papaconstantopoulos, M. J. Mehl, D. Finkenstadt, and G.
 28 Evangelakis, J. Alloy. Compd. **483**, 627 (2009).
 29 T. A. Beu, J. Onoe, and K. Takeuchi, Eur. Phys. J. D **17**, 205 (2001).
 30 J. Cai, R. F. Bie, X. M. Tan, and C. Lu, Physica B **344**, 99 (2004).
 31 D. Finkenstadt, G. Pennington, and M. J. Mehl, Phys. Rev. B **76**, 121405 (2007).
 32 D. A. Papaconstantopoulos and W. E. Pickett, Phys. Rev. B **57**, 12751 (1998).
 33 Mazin, II, D. A. Papaconstantopoulos, and D. J. Singh, Phys. Rev. B **61**, 5223
 34 (2000).
 35 D. A. Papaconstantopoulos, M. J. Mehl, and M. D. Johannes, Phys. Rev. B **82**,
 054503 (2010).
 36 C. Kittel, *Introduction to solid state physics* (Wiley, New York, 1996).
 37 D. A. Papaconstantopoulos and M. J. Mehl, J. Phys.-Condes. Matter **15**, R413
 38 (2003).
 39 O. K. Andersen, Phys. Rev. B **12**, 3060 (1975).
 40 S. H. Wei and H. Krakauer, Phys. Rev. Lett. **55**, 1200 (1985).
 41 M. P. Allen and D. J. Tildesley, *Computer simulation of liquids* (Clarendon,
 42 Oxford, 1989).
 43 D. D. Fitts, *Principles of quantum mechanics as applied to chemistry and
 44 chemical physics* (Cambridge University Press, Cambridge, U.K. ; New York,
 45 1999).
 46 E. A. Carter, Science **321**, 800 (2008).
 47 X. Z. Wu, R. Wang, and S. F. Wang, Appl. Surf. Sci. **256**, 3409 (2010).
 48 T. Kenichi, Phys. Rev. B **60**, 6171 (1999).
 49 G. Steinle-Neumann, L. Stixrude, and R. E. Cohen, Phys. Rev. B **63**, 054103
 50 (2001).
 51 M. Sigalas, D. A. Papaconstantopoulos, and N. C. Bacalis, Phys. Rev. B **45**, 5777
 52 (1992).
 53 X. W. Sha and R. E. Cohen, Phys. Rev. B **81**, 094105 (2010).
 54 G. Simmons and H. Wang, *Single crystal elastic constants and calculated
 55 aggregate properties: a handbook* (M.I.T. Press, Cambridge, Mass., 1971).
 56 U. Wedig, M. Jansen, B. Paulus, K. Rosciszewski, and P. Sony, Phys. Rev. B **75**,
 57 205123 (2007).
 B. M. Klein and R. E. Cohen, Phys. Rev. B **45**, 12405 (1992).
 P. Giannozzi, et al., J. Phys.-Condes. Matter **21**, 395502 (2009).
 H. T. Stokes and L. L. Boyer, (2002).
 B. Dorner, A. A. Chernyshov, V. V. Pushkarev, A. Y. Romyantsev, and R. Pynn,
 J. Phys. F: Metal Phys. **11**, 365 (1981).
 S. Klotz and M. Braden, Phys. Rev. Lett. **85**, 3209 (2000).
 X. W. Sha and R. E. Cohen, Phys. Rev. B **74**, 214111 (2006).
 H. K. Mao, et al., Science **292**, 914 (2001).
 L. M. Peng, G. Ren, S. L. Dudarev, and M. J. Whelan, Acta Crystallogr. Sect. A
52, 456 (1996).
 P. D. Pathak and R. J. Desai, Phys. Status Solidi A-Appl. Res. **62**, 625 (1980).
 D. E. Gray, *American institute of physics handbook* (McGraw-Hill, New York,
 1972).

- ⁵⁸ B. T. A. McKee, Triftsh, auml, W. user, and A. T. Stewart, Phys. Rev. Lett. **28**, 358 (1972).
- ⁵⁹ W. Triftshäuser, Phys. Rev. B **12**, 4634 (1975).

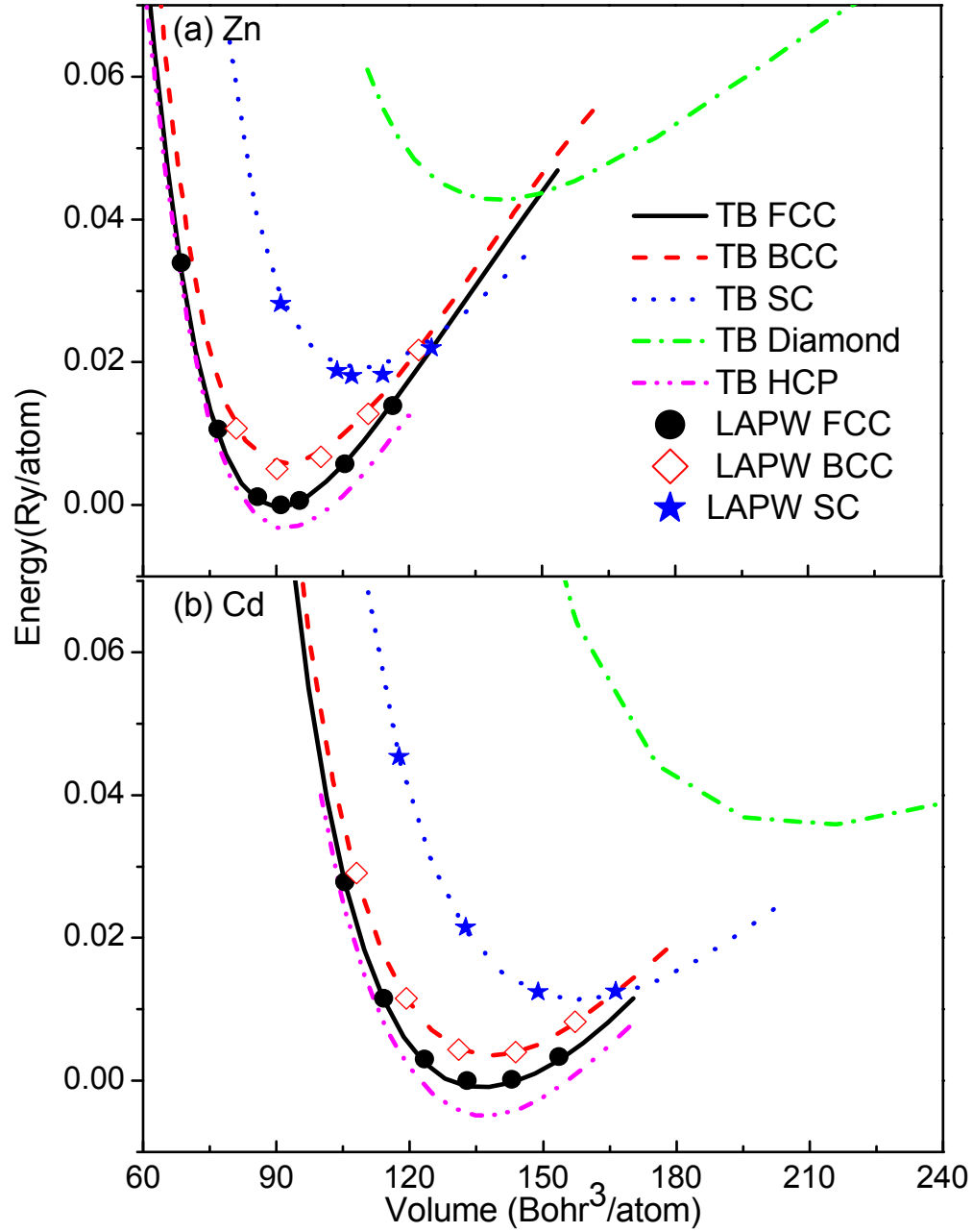


Fig. 1 The tight-binding total energies (lines) of fcc, bcc, hcp, simple cubic, and diamond structures of Zn (a) and Cd (b) as functions of atomic volume, in comparison to the first-principles LAPW results (symbols) of fcc, bcc, and simple cubic structures used in the development of tight-binding Hamiltonians. The tight-binding hcp results here are not directly comparable to the LAPW values used in the fitting due to different c/a ratios.

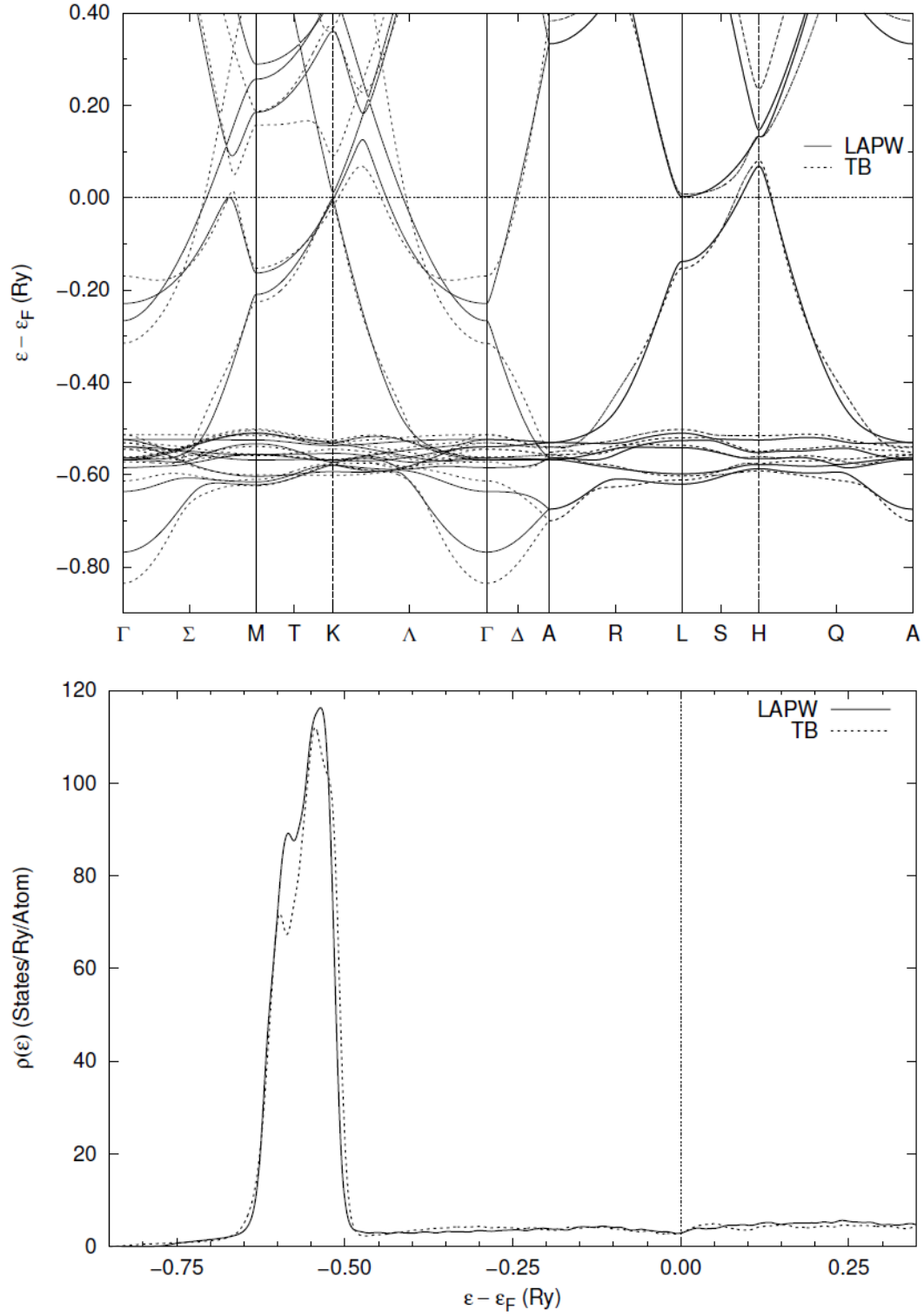


Fig. 2 The tight-binding band structure and electronic density of states of hcp Zn at the ambient experimental equilibrium volume agree well with first-principles LAPW results.

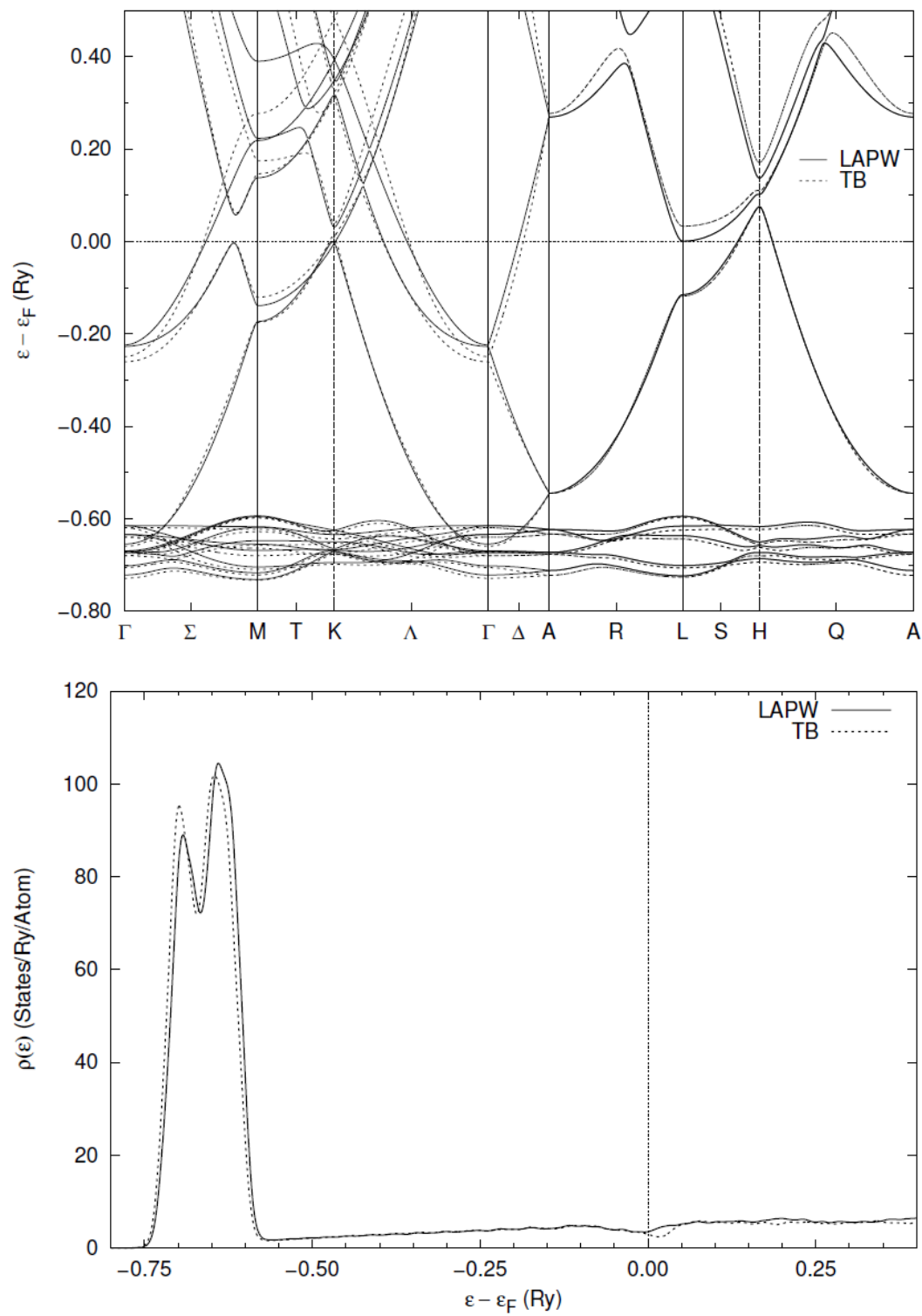


Fig. 3 Same as Fig. 2, but for hcp Cd.

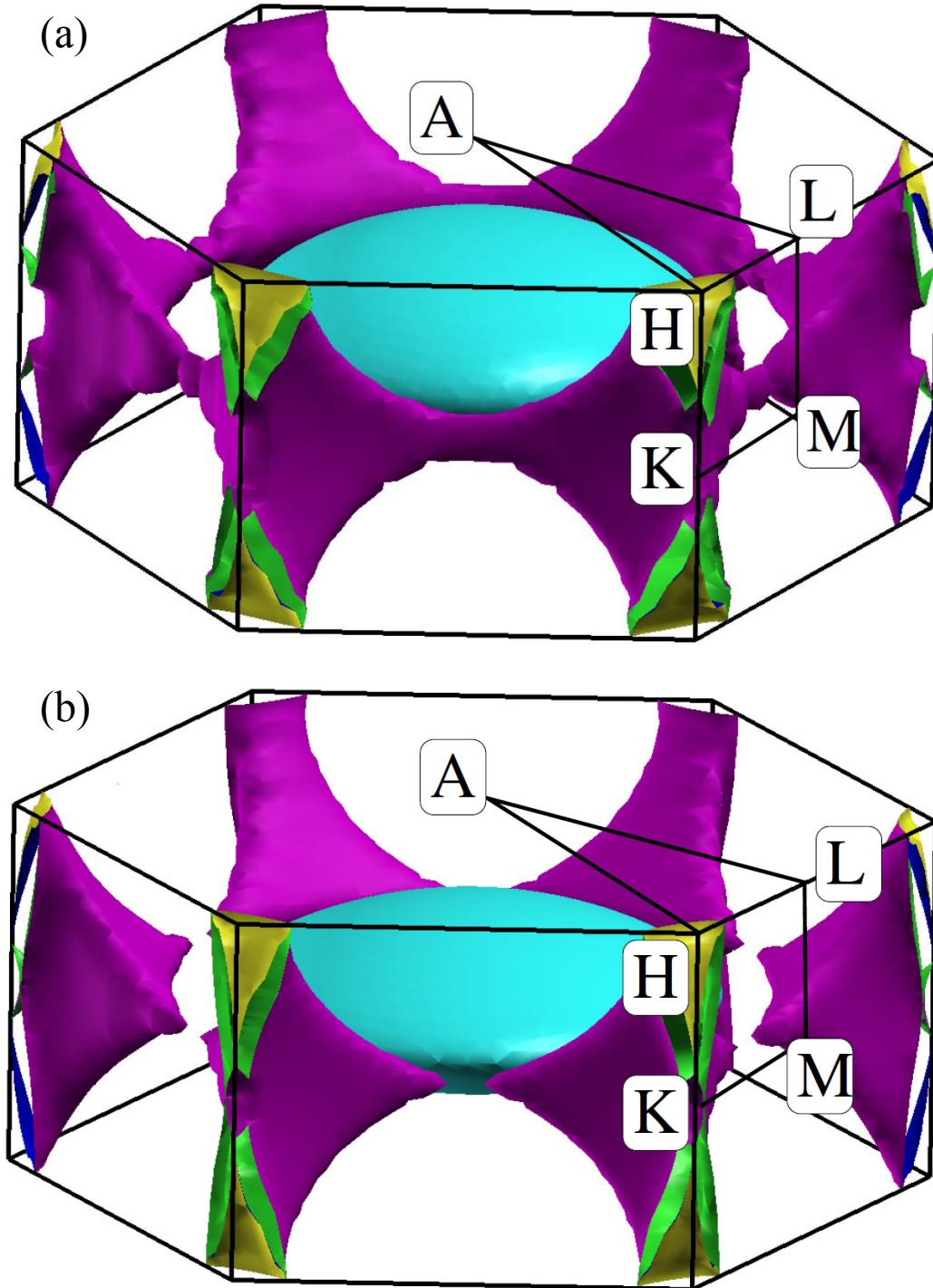


Fig. 4 The tight-binding (a) and LAPW (b) calculated Fermi surfaces for hcp Zn. There are three bands, one forming pockets around the upper and lower parts of each corner (the H point) (green/yellow); the second (purple/blue) filling the entire corner (the K -H line) and maybe connecting the corners; and the third, in light blue, filling the zone center.

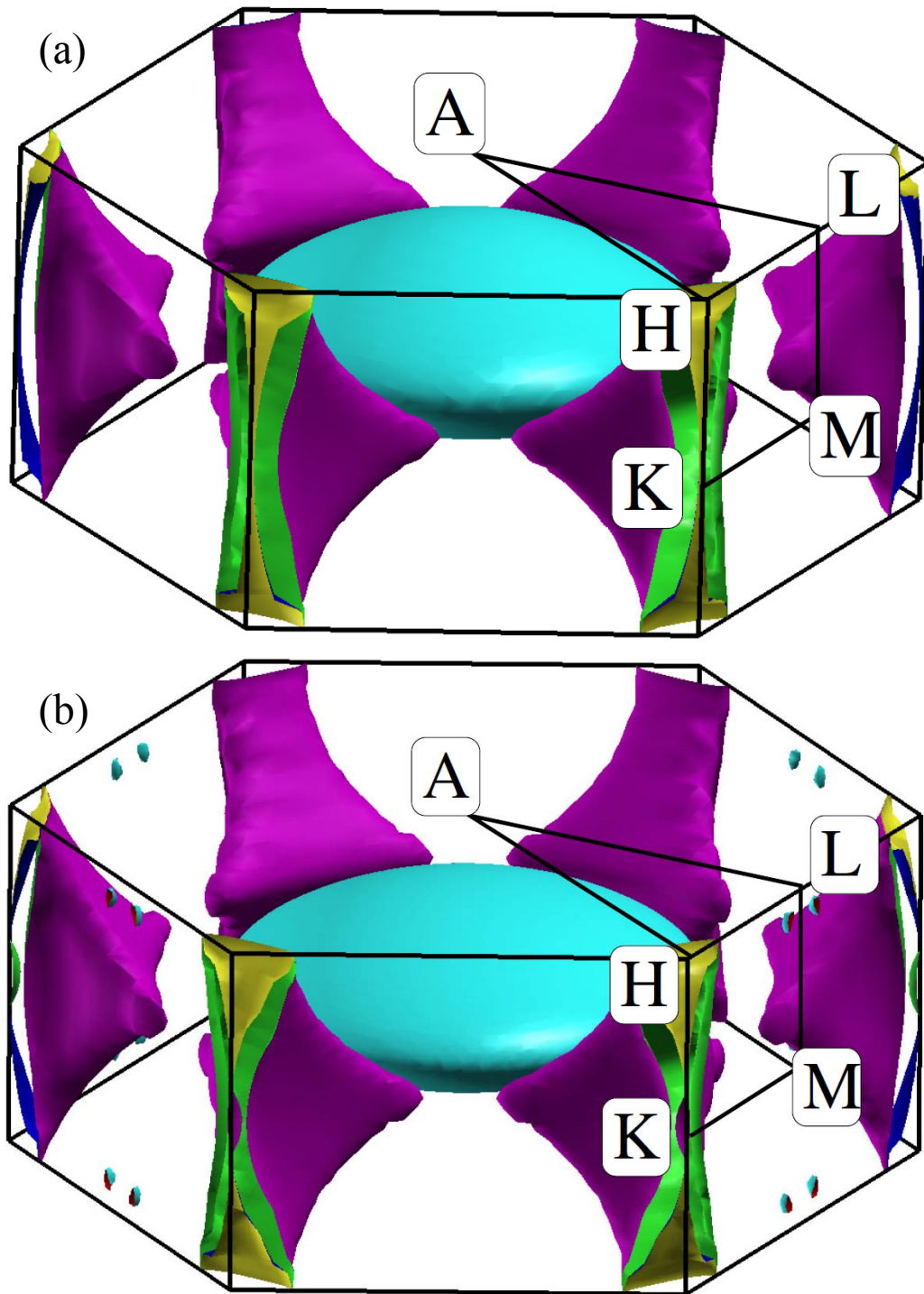


Fig. 5 same as Fig. 4, but for hcp Cd.

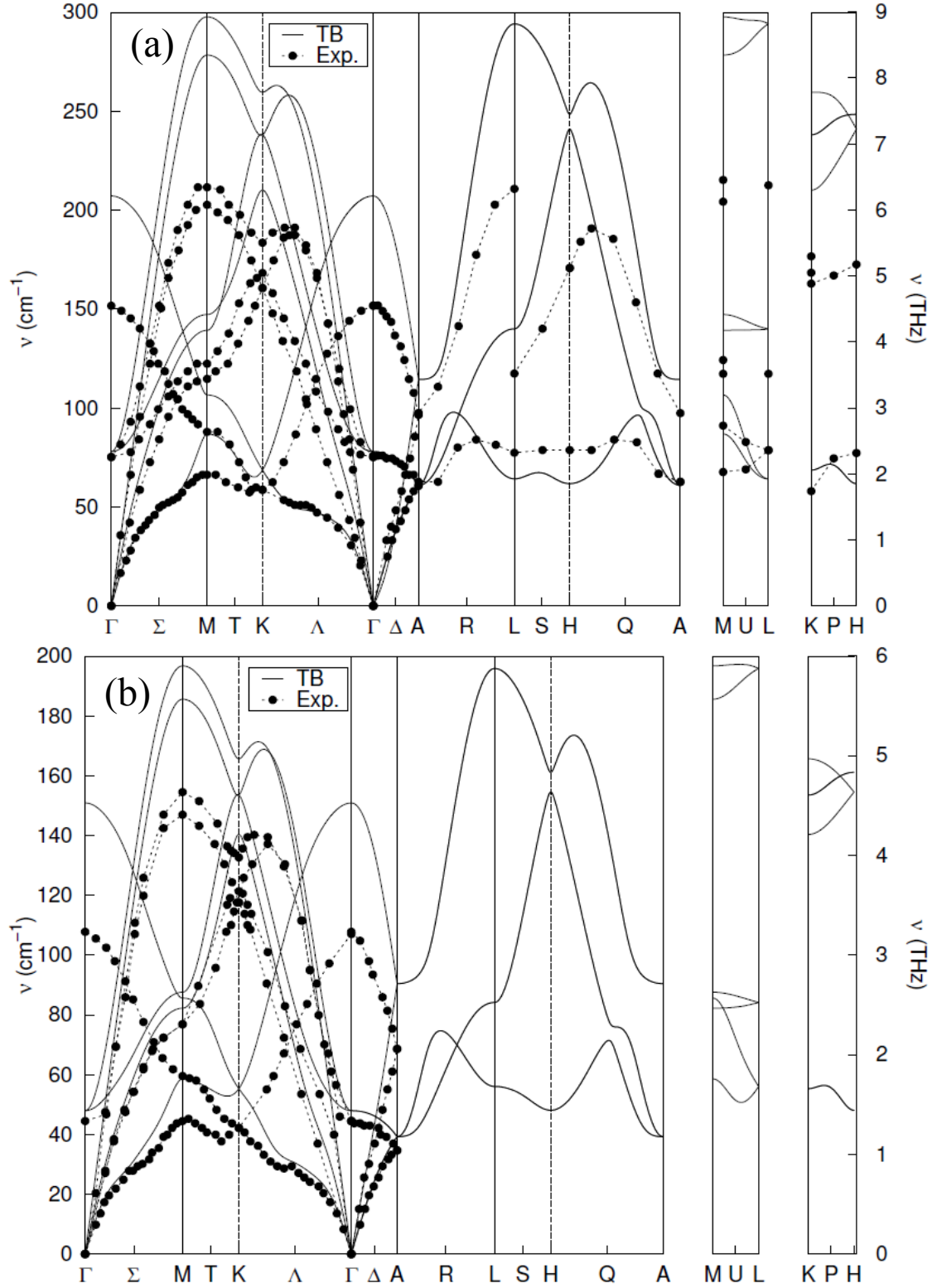


Fig. 6 The calculated phonon dispersion of hcp Zn (a) and Cd (b), in comparison to the inelastic neutron scattering measurements (Ref. ⁵¹).

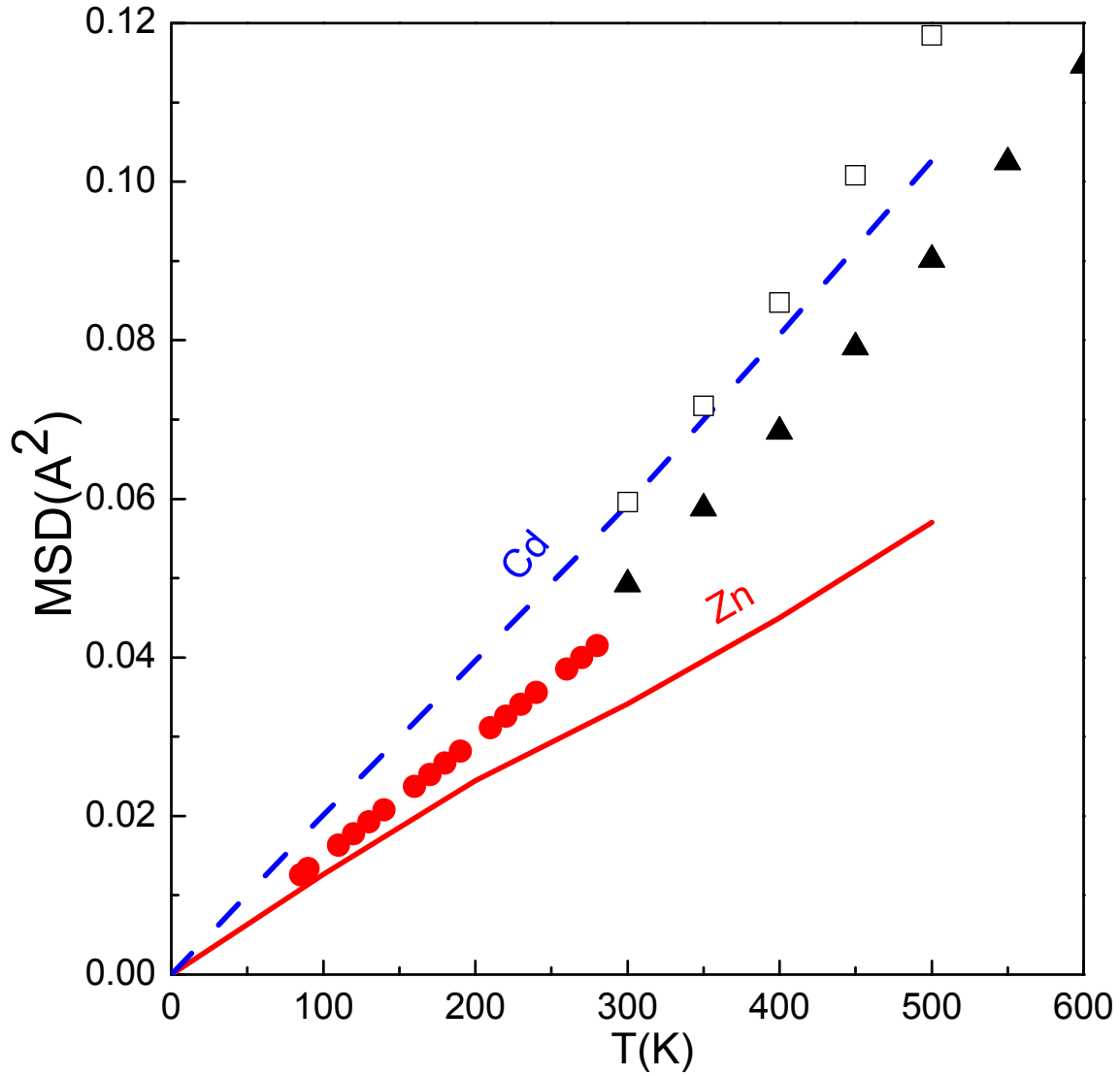


Fig. 7 The temperature dependence of the atomic mean square displacements for hcp Zn (solid line) and Cd (dash line) calculated from tight-binding molecular dynamics simulations, in comparison to the experimental data derived from the Debye-Waller factor measurements (Zn, filled circles, Ref. ⁵⁵, filled triangles, Ref. ⁵⁶; Cd, open squares, Ref. ⁵⁶).

Table I Tight-binding coefficients for Zn and Cd, generated by fitting to the first-principles LAPW total energies and band structures of bcc, fcc, hcp and simple cubic structures.

Zn				
On-site parameters ($\lambda=1.469991$ a.u. ^{-1/2})				
$\rho_i = \sum_j \exp(-\lambda^2 R_{ij}) F_c(R_{ij})$ $h_\ell = a_\ell + b_\ell \rho^{\frac{2}{3}} + c_\ell \rho^{\frac{4}{3}} + d_\ell \rho^2$				
ℓ	a_ℓ	b_ℓ	c_ℓ	d_ℓ
<i>s</i>	0.22328	33.46771	-5376.929237	530223.036806
<i>p</i>	0.697637	10.633128	-4414.114916	858194.489409
<i>d</i>	-0.032554	-1.145394	339.451793	-73547.97693
Hopping terms				
$P_\gamma(R) = \sum_j (e_\gamma + f_\gamma R + g_\gamma R^2) \exp[-q_\gamma^2 R] F_c(R)$				
γ	e_γ	f_γ	g_γ	q_γ
<i>ss</i> σ	2.630211	-1.072291	0.049662	0.800106
<i>sp</i> σ	1.702888	0.371463	0.119067	1.022335
<i>pp</i> σ	-0.138547	0.077519	0.001158	0.660035
<i>pp</i> π	-3.547105	0.662968	0.02738	0.788917
<i>sd</i> σ	-0.088475	-0.139397	0.00354	0.834245
<i>pd</i> σ	-0.480234	0.082434	0.004016	0.839235
<i>pd</i> π	9.892114	0.247499	-0.585076	0.981195
<i>dd</i> σ	1.573334	0.054652	-0.204651	1.042584
<i>dd</i> π	5.528614	-0.835957	0.046933	1.037825
<i>dd</i> δ	-160.313912	-9.176101	7.146619	1.358961
Overlap terms				
$S_\gamma(R) = \sum_j (\delta_\gamma + t_\gamma R + r_\gamma R^2) \exp[-u_\gamma^2 R] F_c(R)$				
γ	δ_γ	t_γ	r_γ	u_γ
<i>ss</i> σ	-40.426164	13.824170	0.064994	1.063141

$sp\sigma$	8.349221	-3.406862	-0.124509	0.895341
$pp\sigma$	-0.758428	-0.047789	0.002815	0.549763
$pp\pi$	1.905233	-0.050823	-0.008351	0.666625
$sd\sigma$	5.482247	-1.123358	-0.072468	0.848286
$pd\sigma$	1.096869	0.443588	-0.23008	0.860846
$pd\pi$	317.522047	-47.939737	-6.193006	1.188616
$dd\sigma$	2179.46986	466.04847	-186.821306	1.442683
$dd\pi$	-2.729519	0.11063	-0.093612	1.041364
$dd\delta$	20.891994	0.38954	-0.571871	1.00681

Cd

On-site parameters ($\lambda=1.605663$ a.u.^{-1/2})

$$\rho_i = \sum_j \exp(-\lambda^2 R_{ij}) F_C(R_{ij})$$

$$h_\ell = a_\ell + b_\ell \rho^{\frac{2}{3}} + c_\ell \rho^{\frac{4}{3}} + d_\ell \rho^2$$

ℓ	a_ℓ	b_ℓ	c_ℓ	d_ℓ
s	0.363794	86.10881	-76791.192088	108436393.485
p	0.867613	-127.036573	133590.464111	124813010.82
d	-0.06385	15.238177	-20740.893262	-2843236.2717

Hopping terms

$$P_\gamma(R) = \sum_j (e_\gamma + f_\gamma R + g_\gamma R^2) \exp[-q_\gamma^2 R] F_c(R)$$

γ	e_γ	f_γ	g_γ	q_γ
$ss\sigma$	5.724943	-6.601102	0.015762	1.061474
$sp\sigma$	0.245014	-0.02487	0.000418	0.542236
$pp\sigma$	-31.355628	5.972695	-0.038353	0.894364
$pp\pi$	18.204678	-0.142384	-0.550664	1.01025
$sd\sigma$	-380.682071	88.930014	-0.168741	1.212736
$pd\sigma$	15.707529	-3.273015	0.003657	0.890509
$pd\pi$	2.011892	0.250708	0.027848	1.073848
$dd\sigma$	58.263161	-19.937689	0.347991	1.163757
$dd\pi$	11.827992	-1.5099	0.017756	1.013595
$dd\delta$	-4.736575	0.623097	-0.001169	1.073331

Overlap terms				
$S_\gamma(R) = \sum_j (\delta_\gamma + t_\gamma R + r_\gamma R^2) \exp[-u_\gamma^2 R] F_c(R)$				
γ	δ_γ	t_γ	r_γ	u_γ
<i>ss</i> σ	-0.392718	0.470493	-0.033283	0.667106
<i>sp</i> σ	59.630549	-15.443898	-0.204783	0.973806
<i>pp</i> σ	6.28926	-3.547458	-0.134306	0.90149
<i>pp</i> π	4.911012	-0.602315	0.006926	0.754477
<i>sd</i> σ	11.256193	-0.07029	-0.410407	1.030123
<i>pd</i> σ	133.598176	-11.940802	-3.109452	1.097928
<i>pd</i> π	-33.085745	3.64351	1.411897	1.047261
<i>dd</i> σ	4.848817	0.438177	-0.121407	1.031423
<i>dd</i> π	-7.338715	-0.233211	0.021357	1.002701
<i>dd</i> δ	-26.229872	2.851133	0.782012	1.096638

Table II The calculated tight-binding total energies of Zn in 26 different crystal structures. Tight-binding calculations correctly predict that hcp is the equilibrium structure, and its energy E_0 is the lowest among all the structures examined.

structure	name	# atoms	V(bohr ³ /atom)	E-E ₀ (Ry/atom)
A3	hcp	2	91.23	0.00000
C19	α -Sm	3	91.75	0.00063
A3'	dhcp	4	91.62	0.00079
A13	β -Mn	20	93.97	0.00093
A _a	α -Pa (c/a = 0.77)	1	93.47	0.00129
A10	α -Hg (51.5°)	1	93.77	0.00246
A1	fcc	1	90.45	0.00247
A12	α -Mn	29	92.60	0.00418
A _b	β -U	30	91.46	0.00458
A7	α -As	2	98.39	0.00481
A15	A15	8	91.70	0.00539
A11	α -Ga	4	99.14	0.00550

A16	α -S	32	97.89	0.00745
A _f	simple hexagonal	1	101.96	0.00760
A8	γ -Se	3	101.99	0.00769
A2	bcc	1	91.90	0.00848
C32	ω	3	93.34	0.00913
bct5	bct 5	2	99.34	0.00968
A5	β -Sn	2	104.43	0.01705
A _h	simple cubic	1	108.63	0.02181
hR12	α -B	12	122.10	0.02199
d2h	2H diamond	4	123.53	0.02990
A9	graphite	4	119.08	0.03511
A4	diamond	2	140.29	0.04553
E2 ₁	perovskite	5	128.76	0.05067
D0 ₉	ReO ₃	4	173.36	0.06615

Table III Same as Table II, but for Cd.

structure	name	# atoms	V(bohr ³ /atom)	E-E ₀ (Ry/atom)
A3	hcp	2	136.23	0.00000
C19	α -Sm	3	136.74	0.00059
A3'	dhcp	4	136.78	0.00080
A _a	α -Pa (c/a = 0.76)	1	139.19	0.00133
A10	α -Hg (53.0°)	1	137.69	0.00202
A1	fcc	1	136.33	0.00323
A15	A15	8	138.05	0.00342
A13	β -Mn	20	141.25	0.00379
A _b	β -U	30	137.76	0.00423
A12	α -Mn	29	139.59	0.00518
A7	α -As	2	143.71	0.00711
A11	α -Ga	4	145.29	0.00756

A2	bcc	1	137.99	0.00837
bct5	bct 5	2	148.61	0.00840
A16	α -S	32	146.31	0.00849
C32	ω	3	141.34	0.00869
A8	γ -Se	3	149.32	0.01157
A _f	simple hexagonal	1	149.38	0.01160
A5	β -Sn	2	151.81	0.01399
hR12	α -B	12	158.72	0.01408
A _h	simple cubic	1	157.49	0.01591
d2h	2H diamond	4	190.37	0.02893
A9	graphite	4	177.19	0.03081
A4	diamond	2	209.54	0.04040
E2 ₁	perovskite	5	187.21	0.05024
D0 ₉	ReO ₃	4	298.49	0.06042

Table IV The tight-binding calculated bulk and elastic moduli for hcp Zn and Cd at the ambient experimental equilibrium volume are in reasonable agreement with experimental measurements (⁴⁶).

elastic moduli (GPa)				
	hcp Zn		hcp Cd	
	TB	experiment	TB	experiment
C ₁₁	168.52	179.09	134.37	129.23
C ₁₂	27.99	37.50	47.35	39.99
C ₁₃	28.92	55.40	33.66	40.95
C ₃₃	43.17	68.80	62.45	56.68
C ₄₄	24.04	45.95	22.24	24.20

C_{66}	70.27	70.80	43.51	44.62
B	40.74	66.09	52.81	52.51

Table V The tight-binding calculated linear coefficients of thermal expansion for hcp Cd and Zn both agree with experiment⁵⁷.

element	linear thermal expansion coefficient ($\times 10^{-5} \text{ K}^{-1}$)	
	TB	experiment
Zn	1.50	3.01(a:1.30, c: 6.43)
Cd	2.43	3.13(a: 1.98, c: 5.43)

Table VI The tight-binding calculations underestimate the vacancy formation energy for hcp Zn and overestimate the value for hcp Cd, both by ~ 0.30 eV, in comparison to the positron annihilation measurements (⁵⁸).

vacancy formation energy (eV)						
supercell	# atoms	# k-points	hcp Zn		hcp Cd	
			unrelaxed	relaxed	unrelaxed	relaxed
4x4x4	128	32	0.428	0.218	0.951	0.617
		48	0.475	0.272	0.971	0.643
		72	0.494	0.295	1.032	0.708
		108	0.491	0.291	1.033	0.709
5x5x5	250	32	0.447	0.214	1.100	0.740
		48	0.480	0.248	1.086	0.732
		72	0.454	0.222	1.049	0.689
		108	0.487	0.258	1.049	0.690
experiment			0.52		0.39	